Mon. Not. R. Astron. Soc. **000**, 000–000 (0000) Printed 31 July 2014 (MN LATEX style file v2.2)

Dust Formation in the Presence of Photons I: Evaporation Rates for Small Dust Grains

C. S. Kochanek[1,2]
[1] *Department of Astronomy, The Ohio State University, 140 West 18th Avenue, Columbus OH 43210*
[2] *Center for Cosmology and AstroParticle Physics, The Ohio State University, 191 W. Woodruff Avenue, Columbus OH 43210*

arXiv:1407.7856v1 [astro-ph.SR] 29 Jul 2014

31 July 2014

ABSTRACT
The temperature of newly forming dust is controlled by the radiation field. As dust forms around stars, stellar transients, quasars or supernovae, the grains must grow through a regime where they are stochastically heated by individual photons. Since evaporation rates increase exponentially with temperature while cooling times decrease only as a power law, the evaporation rates for these small grains are dominated by the temperature spikes. We calculate effective evaporation temperatures for a broad range of input spectra that are encapsulated in a series of simple interpolation formulae for both graphitic and silicate grains. These can be easily used to first determine if dust formation is possible and then to estimate the radius or time at which it commences for a broad range of radiation environments. With these additional physical effects, very small grains may form earlier than in standard models of AGB winds. Even for very high mass loss rates, the hottest stars that can form dust are G and F stars particularly in the case of silicate dusts. For hotter stars, the higher fluxes of ultraviolet photons prevent dust formation. Thus, episodic dust formation by OH/IR stars and LBVs is primarily driven by fluctuations in their apparent temperatures rather than changes in luminosity or mass loss rates.

Key words: dust – stars: circumstellar matter – stars: AGB and post-AGB – stars: mass loss – stars: winds, outflows

1 INTRODUCTION

Dust formation and destruction is crucial to interpreting a broad range of astrophysical phenomena including stellar winds, stellar transients, supernovae and quasars. In the laboratory, particle formation and growth is simply a collisional process because both the temperature and the growth rates are determined by collisions. Radiation is unimportant because the densities are high ($n \sim 10^{19}$ cm^{-3}) and the (radiation) temperatures are low ($T \lesssim 2000$ K). In most astronomical contexts, however, the reverse is true – the densities are low ($n \lesssim 10^{10}$ cm^{-3}) and the radiation temperatures are high ($T \gtrsim 2000$ K). In these circumstances, particles grow by collisions but the grain temperatures, and hence the evaporation rates, are controlled by the radiation field.

Dust formation can be viewed as having two phases, nucleation and growth (see, e.g., the reviews by Salpeter 1977, Gail & Sedlmayr 2013). The distinction is that there is generally a "critical cluster" size or number (a_{min}, N_{min}), below which a grain will be unstable to returning to its simpler starting components ("monomers") and above which it becomes a stable grain that will continue to grow as it collides with more "monomers" or other grains. Nucleation theory predicts the rate of formation of critical clusters based on the thermodynamics of the gas, but it does so poorly, and nucleation rates at fixed temperature are generally exponentially uncertain (e.g., Wölk et al. 2002). This is exacerbated in astrophysical flows by the very long collision time scales (e.g., Donn & Nuth 1985). In expanding flows, however, the temperature steadily drops and the supersaturation of the vapor phase steadily rises, making a failure to nucleate exponentially unlikely even if the rate at any given temperature is very uncertain. Once grains nucleate and start to grow, their final sizes are determined by kinetics.

As grains try to grow, they must pass through a phase where the number of constituent particles is small, $10 \lesssim N \lesssim 100$, and the specific heat of the grain is low. Such small grains can be stochastically heated to very high temperatures by individual soft ultraviolet (UV) photons, as was originally discussed in the context of the stochastic heating of grains in the interstellar medium (e.g., Sellgren 1984, Draine & Anderson 1985, Desert et al. 1986, Guhathakurta & Draine 1989), the destruction of small grains and polycyclic aromatic hydrocarbons (PAH) near active galactic nuclei (AGN, e.g., Voit 1991, Voit 1992), and dust formation by novae (Johnson et al. 1993). Both

© 0000 RAS

the shorter wavelength fluxes and the evaporation rates of small grains are dominated by the short duration temperature spikes because the emission or evaporation rises exponentially with grain temperature while the time spent at the highest temperatures drops only as a power-law.

Stochastic heating is rarely mentioned in the context of dust formation. For example, many studies of dust formation by supernovae ignore radiative heating entirely and set the grain temperature to that of the gas (e.g., Kozasa et al. 1991, Todini & Ferrara 2001, Nozawa et al. 2003, Bianchi & Schneider 2007). Others, such as Dwek (1988) for SN, Clayton & Wickramasinghe (1976) for novae and Lefevre (1979) for stars and novae set the grain temperature to be in equilibrium with the absorbed flux. A few studies such as Guhathakurta & Draine (1989) for dust in the ISM, Johnson et al. (1993) for dust formation in novae, Cherchneff & Dwek (2009) for the effects of hard photons on the pre-cursor chemistry to dust formation in SN, and Keith & Lazzati (2011) for the growth of small carbonaceous grains have considered the role of stochastic heating.

In most astrophysical contexts, gas collisions are unimportant to the thermodynamic state of a grain.[1] The grain heats and cools by absorbing and emitting photons. Small grains are also thermally isolated in the sense that the grain experiences no collisions with gas particles over the time scale needed for the grain to cool after absorbing a photon (Guhathakurta & Draine 1989, Johnson et al. 1993). This makes dust formation extremely sensitive to the hardness of the radiation field, and provides a natural explanation of why dust fails to form around hot stars even for very high mass loss rates (Kochanek 2011). Around the very cool stars that are the focus of most studies of dust formation (e.g., Rowan-Robinson & Harris 1983, Gauger et al. 1990, or more recently, Nanni et al. 2013 and Ventura et al. 2014), the effect becomes relatively unimportant because the stellar temperatures are too low to drive strong stochastic heating. However, for dust formation around hotter stars, stellar transients, novae, supernovae and AGN, these radiative effects cannot be neglected.

Without stochastic heating, dust formation in outflows seems almost inevitable provided there is a mechanism to initiate the outflow (see, e.g., the review by Lafon & Berruyer 1991). For simplicity, consider an N particle grain near a source of luminosity L_* emitting photons of energy $E_\gamma = kT_\gamma$ and ignoring Planck factors. In equilibrium, the grain has a black body temperature of $T_{bb} = (L/16\pi\sigma r^2)^{1/4}$ when it is a distance r from the source. Evaporation rates depend exponentially on temperature, $\propto \exp(-T_c/T_{bb})$, where kT_c is the binding energy of particles to the grain (e.g., Lefevre 1979, Guhathakurta & Draine 1989), so evaporation rates drop exponentially with distance since $T_c/T_{bb} \propto r^{1/2}L^{-1/4}$. Collisional growth rates are proportional to density, so in an expanding (wind) flow the growth rate also declines with distance but only as a power law, $\propto r^{-2}$. At some radius that is only logarithmically dependent on the spectrum or the density, the collisional growth rate exceeds the evaporation rate and the grain will begin to grow unless the densities are so low that there is no probability of experiencing any collisions. All sufficiently dense flows should form dust.

Stochastic heating fundamentally changes the scaling of the evaporation rate with distance. Suppose that a grain containing N particles has time to completely cool between photon absorptions. When the grain absorbs a photon, it is heated by temperature $\Delta T = T_\gamma/c_V N$ where $c_V \sim$ 2-3 is the specific heat of the grain. If $\Delta T \gtrsim T_{bb}$, all evaporation occurs at the temperature ΔT set by the photon energy rather than the black body temperature T_{bb} set by the photon flux. However, the radiative cooling time scale, $t_{cool} = c_V N k \Delta T/4\pi a^2 \sigma \Delta T^4$, for a grain of radius a is short compared to the rate of photon absorptions, $R = L\pi a^2/4\pi r^2 E_\gamma$, leading to an average evaporation rate of $\propto \exp(-T_c/\Delta T) t_{cool} R = \exp(-T_c/\Delta T) L/r^2 \Delta T^4$. The term in the exponential is constant, so the evaporation rate now drops with the same r^{-2} radial power law as the collisional growth rates and distance does not affect the balance between evaporation and growth. Only modest photon energies are needed to drive this process for small grains, since photons of energy $E_\gamma \simeq 0.2 c_V N$ eV will heat a grain by 2000 K and all but the coldest stars and transients produce large numbers of such photons.

Our original interest in this question comes from the properties of ejecta around Luminous Blue Variables (LBVs), massive hot stars with dense winds ($\dot{M} \sim 10^{-5}$ to $10^{-4} M_\odot$/year) that are not presently forming dust yet are frequently surrounded by massive dusty shells of material (see the reviews by Humphreys & Davidson 1994, Vink 2012). The most recent example is η Car, but there are some 10(s) of examples in the Galaxy. In Kochanek (2011) we argued that this could be explained by stochastic heating of small grains. Despite the density of their present day winds, the abundance of soft ultraviolet photons prevents dust formation. In eruption, the wind becomes optically thick, leading to a pseudo-photosphere that is much cooler (Davidson 1987), and this allows dust to form. For dust formation, this change in radiation temperature is more important than the increase in wind density, although the higher wind density ($\gtrsim 10^{-3} M_\odot$/year) required to produce the pseudo-photosphere certainly accelerates the growth of the grains. Thus, the effects of stochastic heating provide a natural explanation for hot stars surrounded by young ($< 10^4$ year), dusty shells.

More generally, the nature of the radiation field is likely important for dust formation in all astrophysical scenarios where the radiation temperature is high compared to the dust evaporation temperature. This includes LBVs, OH/IR stars, novae, supernovae, other stellar transients (e.g., supernova "impostors", and pre-super mass loss events) and quasars. In Kochanek (2011) we simply compared the collision rates to the soft UV photon absorption rate. Here, in §2 we explicitly calculate the stochastic heating of small grains to obtain interpolation formulae that can be used in any context. We discuss the differences between various treatments of the radiative heating of small grains in §3. In §4 we show how these results apply to steady winds as a function of stellar temperature and mass loss rates. In §5 we

[1] The critical density for collisions to dominate over radiation given grain and gas temperatures of T_{g3} and T_{gas3} in units of 1000 K is

$$n \gtrsim 10^{15} \frac{Q(T_g) T_{g3}^4}{|T_{gas3} - T_{g3}| T_{gas3}^{1/2}} \ \mathrm{cm}^{-3}. \quad (1)$$

discuss a few of the implications for dust formation in near AGB stars, OH/IR stars and long-lived LBV eruptions such as the Great Eruption of η Carinae. Detailed discussions of dust formation in shorter transients, supernovae and quasars will follow separately.

2 DUST FORMATION

We are generally considering dust formation near a star of mass $M_* = 10M_{*10}M_\odot$, luminosity $L_* = 10^4 L_{*4}L_\odot$, temperature $T_* = 10^4 T_{*4}$ K and radius $R_* = L_*/4\pi\sigma T_*^4$, forming dust in a wind with mass loss rate $\dot{M} = 10^{-4}\dot{M}_4 M_\odot$/year and velocity $v_w = 10v_{w10}$ km/s or scaled by the stellar escape speed

$$v_w = \beta\sqrt{\frac{2GM_*}{R_*}} \simeq 338\beta M_{*10}^{1/2} T_{*4} L_{*4}^{-1/4} \text{ km/s}. \quad (2)$$

For a wind we use the simple constant velocity density profile

$$\rho = \frac{\dot{M}}{4\pi v_w r^2} \quad (3)$$

of which mass fraction $X = 0.01X_2$ is comprised of the condensible species (X can be much higher for (super)nova ejecta). Dust forms in grains of radius a containing $N = 4\pi a^3\rho_b/3m_0$ particles where ρ_b is the bulk density and m_0 is the (average) mass of a monomer. Following Guhathakurta & Draine (1989), we use $m_0 = 12m_p$ ($20m_p$) and a bulk density of $\rho_{bulk} = 2.2$ (3.5) g cm^{-3} for graphitic (silicate grains). Note that the ratio ρ_{bulk}/m_0 is essentially identical for the two compositions, so $a = 0.00013N^{1/3}\mu$m in both cases. We will be discussing very small ($10 \le N \le 100$) "grains", and we will discuss the applicability of using bulk properties as we proceed. We use the dust cross sections and Planck averaged cross sections from Draine & Lee (1984) and Laor & Draine (1993) extending them below 0.001μm with $Q \propto a$ and above 10μm with Q constant.

Our objective is to determine the conditions under which a small grain containing N monomers can grow given the density and radiation environment. Growth is set by the balance between collisional gains and evaporative losses. In these early phases, we can focus on growth by collision with monomers, so the growth rate is

$$\left(\frac{dN}{dt}\right)_c = R_c = \frac{\alpha\pi a^2 X\rho v_c}{m_0} \quad (4)$$

where v_c is the collision velocity and $\alpha \le 1$ is the "sticking probability" (e.g., Kwok 1975, Deguchi 1980, Gail et al. 1984, Gail & Sedlmayr 1988). When a monomer condenses onto a grain, the grain is heated by the energy of condensation, increasing the probability of then evaporating a monomer. The sticking probability can be used to model the resulting, net condensation rate and it becomes smaller for smaller grains (Johnson et al. (1993) estimate that $\alpha \simeq 0.6$ for $N = 10$ but only 10^{-4} for $N = 3$) because small grains have fewer vibrational degrees of freedom. We will only consider larger ($N > 10$) grains and we will consider a model in which the effects of condensation and evaporation are included when evolving the grain enthalpy. Thus, we can generally set $\alpha = 1$ since small changes in α are also unimportant compared to the potential range of wind densities. Associated with any flow at radius R, there is also an expansion time, $t_e = R/v_w$. Growth is kinetically limited, in the sense that there are no collisions, if the collision rate is less than the expansion rate, $(dN/dt)_c < t_e^{-1}$.

The collision velocity v_c is a combination of gas temperature, drift velocities and any turbulent velocities. Since the gas is cold, $T_{gas} = 1000T_{gas3}$ K, and the monomers are relatively heavy, the thermal velocities of the monomers are low, $v_{th} \simeq 0.8T_{gas3}^{1/2}$ km/s (one velocity component, carbon). The thermal velocities of the grains are then still lower by $N^{-1/2}$. The grains also drift relative to the gas at velocity

$$v_d = \left(\frac{Q_{rp}(T_*)L_*}{4\pi r^2\rho c}\right)^{1/2}, \quad (5)$$

which is the balance between radiation pressure accelerating the grains and collisional drag from the gas (e.g., Netzer & Elitzur 1993). The radiation pressure Planck factor, Q_{rp}, is roughly equal to the absorption Planck factor $\langle Q_{abs}\rangle$ we use below. If we substitute the density of a wind, then

$$v_d \simeq 0.3\beta^{1/2} L_{*4}^{3/8} M_{*10}^{1/4} \hat{Q}_{rp}^{1/2} T_{*4}^{1/2} \dot{M}_4^{-1/2} N^{1/6} \text{ km/s} \quad (6)$$

where $Q = \hat{Q}(a/\mu m)$ and $\hat{Q}_{rp}(T_*)$ is small for cool stars (0.1-1) and larger for hot stars (10^2).[2] If $v_d \gtrsim v_{crit} \simeq 50$ km/s, sputtering by collisions with the carrier gas will destroy the grain (e.g., Draine 1995). In theory this is possible for very low $\dot{M}$, but at such low wind densities dust growth is already impossible due to kinetics. Like the sticking probability, the dynamic range of v_c is small compared to that of the density, so we will simply scale the collision velocity by $v_c = 1v_{c1}$ km/s.

The formation radius R_f represents the point at which the grain can begin to grow faster than it evaporates, where the grain temperature T_g determines the evaporation rate,

$$\left(\frac{dN}{dt}\right)_e = R_e = -4\pi a^2 R(N, T_g) S(N, T_g). \quad (7)$$

Here $R(N, T_g)$ is the evaporation rate per unit area in thermal equilibrium and $S(N, T_g)$ accounts for the suppression of thermal fluctuations if the grain is thermally isolated from the surrounding gas in the sense that radiative time scales are shorter than collisional time scales (Guhathakurta & Draine 1989). The evaporation rates are modeled as

$$R(N+1, T) = A\exp\left[-B/T\right] \quad (8)$$

with

$$\begin{aligned} A &= 4.6\times10^{30}\alpha \text{ cm}^{-2}\text{ s}^{-1} \quad \text{and} \\ B &= 81200 - 20000(N-1)^{-1/3} \text{ K}, \end{aligned} \quad (9)$$

for graphite and

$$\begin{aligned} A &= 4.9\times10^{31}\alpha \text{ cm}^{-2}\text{ s}^{-1} \quad \text{and} \\ B &= 68100 - 20000(N-1)^{-1/3} \text{ K}, \end{aligned} \quad (10)$$

for silicates where α is the "sticking probability" (Guhathakurta & Draine 1989). Since α appears in both the

[2] For $2600 < T_* < 50000$ K and small grains, they can be approximated as $\ln\hat{Q} \simeq 2.969 + 1.578x - 0.176x^2$ for graphite and $0.600+2.925x+1.141x^2$ ($T_* < 10^4$ K) and $0.600+4.378x-1.118x^2$ ($T_* > 10^4$ K) for silicate where $x = \ln(T_*/10^4)$.

collision and the evaporation rates, we simply set $\alpha = 1$. The suppression factor

$$S(N,T) = \left(\frac{1+\gamma}{\gamma}\right)^b \frac{\Gamma[\gamma f+1]\Gamma[\gamma f+f-b]}{\Gamma[\gamma f-b+1]\Gamma[\gamma f+f]} \quad (11)$$

reduces the rate below that for thermal equilibrium ($R(N,T)$) by the probability of having enough vibrational quanta in the bond holding a surface atom onto the grain given that the number of vibrational quanta is fixed if the grain is in isolation. The grain has $f = 3N-6$ vibrational degrees of freedom with an (assumed) common vibrational energy $\hbar\omega_0 = 0.75k\Theta$ of the Debye temperature ($\Theta = 420$ K for graphite, 470 K for silicates). The quantity $\gamma = U/f\hbar\omega_0$ is the mean number of vibrational quanta per degree of freedom given the internal energy of the grain and $b = kB/\hbar\omega_0$. If $\gamma f - b + 1 \le 0$, then the evaporation is completely suppressed, and this effectively corresponds to the requirement that $U > kB$ before any evaporation is possible. As discussed in §1, the grains are essentially always thermally isolated from the carrier gas on the time scale for cooling after absorbing a photon. Again following Guhathakurta & Draine (1989), the enthalpy of an N atom graphitic grain can be approximated as

$$U_N = \frac{4.15\times10^{-22}(N-2)T^{3.3}\ \mathrm{ergs/atom}}{1+6.51\times10^{-3}T+1.5\times10^{-6}T^2+8.3\times10^{-7}T^{2.3}}, \quad (12)$$

while for silicates

$$U_N = (N-2)(10^{-21}\ \mathrm{ergs/atom})\times \quad (13)$$
$$\begin{cases} 4.43T^3 & T<50 \\ 7.33\times10^5(T/50)^{2.3}-1.80\times10^5 & 50<T<150 \\ 1.23\times10^7(T/150)^{1.68}-3.27\times10^6 & 150<T<500 \\ 1.62\times10^8(T/500)-7.23\times10^7 & 500<T. \end{cases}$$

The energy required to heat a grain to 1500 K is roughly $0.25(N-2)$ eV in both cases, so the flux of 1-10 eV photons controls the importance of stochastic heating, particularly since hydrogen will generally absorb > 13.6 eV photons.

The simplest way to consider particle formation is to view it as completely suppressed as long as the evaporation rate (Equation 7) exceeds the collisional growth rate (Equation 4). Without stochastic heating, the evaporation rate depends on the nature of the incident spectrum because the black body equilibrium temperature

$$\frac{L}{4\pi r^2} = 4\sigma T_{bb}^4 \quad (14)$$

differs from the Planck equilibrium temperature

$$\frac{L\langle Q_{abs}\rangle}{4\pi r^2} = 4\sigma T_g^4 Q_{em}(T_g) \quad (15)$$

where $\langle Q_{abs}\rangle = \int F_\nu Q_{abs}(\nu)d\nu / \int F_\nu d\nu$ depends on the incident radiation spectrum and $Q_{em}(T_g)$ on the grain temperature. Generally $\langle Q_{abs}\rangle$ increases with the radiation temperature and is larger than $Q_{em}(T_g)$, so the grain is hotter than predicted from the black body temperature. Equating the collisional growth (Equation 4) to the evaporation rate (Equation 7), a grain can grow if

$$T_g < B\left[\ln\left(\frac{4Am_0S}{X\rho v_c}\right)\right]^{-1} \quad (16)$$
$$\simeq B\left[50+\ln\left(\frac{SA}{10^{31}}\frac{10^5}{n_{cond}}\frac{\mathrm{km/s}}{v_c}\right)\right]^{-1}$$

where the number density of the condensible species is $n_{cond} = X\rho/m_0$. This basically leads to a characteristic temperature of order $B/50 \sim 1500$ K because reasonable changes in the variables entering the logarithm do not produce changes that are significant fractions of the leading constant. For example raising the collisional growth rate by 10^5 (e.g., raising n_{cond} from 10^5 to 10^{10} cm^{-3}) only changes the limit from $T_g < B/50$ to $B/38$.

In equilibrium, the thermal evolution is controlled by two effects. The first, familiar effect is radiation balance

$$\frac{dU}{dt} = -4\pi a^2\sigma T_g^4 Q_{em}(T_g) + \frac{L\langle Q_{abs}\rangle\pi a^2}{4\pi r^2}. \quad (17)$$

Here the second term is the mean radiative heating, but we can also treat it stochastically in terms of individual photons. We must also, however, account for the energy associated with adding or evaporating a particle from the grain (e.g., Waxman & Draine 2000),

$$\frac{dU}{dt} = (R_e + R_c)kB \quad (18)$$

where $R_c = (dN/dt)_c > 0$ and $R_e = (dN/dt)_e < 0$ are the condensation (Equation 4) and evaporation (Equation 7) rates, respectively. Since we are searching for the point where evaporation and growth are in balance, the average of this term is zero. However, the heating from particle addition is uncorrelated with grain temperature, while evaporation will preferentially occur when the temperature is high. Thus, high temperature peaks cool faster when we include these terms and, as you add more heat, the evaporation rate increases rather than the mean temperature. These terms will be treated stochastically. As discussed above, it is easily shown that collisions with the carrier gas are generally unimportant to the thermal balance.

Operationally, we carried out the calculations as follows. We treated photons with energy < 0.1 eV as contributing a steady heating term in Equation 17 and computed the cooling curve of a grain $U(t)$ and temperature $T(t)$ in the absence of any stochastic event. We also computed the total number of particles $\Delta N(t)$ evaporated. Given these curves, the remainder of the calculation is simply an iterative procedure with no need for further numerical integration. From the photon spectrum, we can determine the rate of discrete photon absorptions. We work with normalized spectra, $b_\nu = B_\nu / \int B_\nu d\nu$, so the flux of photons of energy $h\nu$ at any radius is $F_\nu = Lb_\nu/4\pi r^2$. Given this photon flux, the rate at which photons are absorbed by the grain is $R_\gamma = \pi a^2 \int F_\nu Q_{abs}(\nu)(h\nu)^{-1}d\nu$. The photon energy E_γ is found by randomly sampling the distribution $\nu^{-1}b_\nu Q(\nu)$. We also have the current evaporation rate R_e and the average capture rate $R_c = \langle R_e\rangle$ which are set to be equal because we are solving for the conditions where they just balance.

The rate of events is then $R = R_\gamma + R_e + R_c$, so the time until the next event is $\Delta t = -R^{-1}\log(1-P)$ where P is a uniform random deviate. Given the current grain enthalpy, $U(t)$, we can follow the tabulated cooling curve to $U(t+\Delta t)$ and the contribution of this time interval to the overall amount of evaporation. Based on the relative rates we can randomly select the next event, and update the enthalpy by adding the energy of the absorbed photon, $U(t+\Delta t)+E_\gamma$, cool by evaporating a monomer, $U(t+\Delta t)-kB$, or heat by capturing a monomer, $U(t+\Delta t)+kB$. We start the grain at its Planck equilibrium temperature and use a "break in"

period to forget this initial condition and bring the capture rate to equal the mean evaporation rate. From the end of the break in period to the end of the calculation we total the evaporations and then divide by the elapsed time to obtain the mean evaporation rate $\langle dN/dt \rangle_e$. Typically we followed 10^7 events.

We tracked five different cases for comparisons:

- Case 1 (Planck equilibrium): thermally coupled grains at the equilibrium temperature and only photons (Equation 7 with $S \equiv 1$ plus Equation 15 and no Equation 18);
- Case 2: thermally isolated grains at the equilibrium temperature and only photons (Equation 7 plus Equation 15 and no Equation 18);
- Case 3: stochastically heated grains that are thermally coupled and only photons (Equation 7 with $S \equiv 1$ plus Equation 17 and no Equation 18);
- Case 4: stochastically heated grains that are thermally isolated and only photons (Equation 7 plus Equation 17, and no Equation 18); and
- Case 5: stochastically heated grains that are thermally isolated with evaporation and capture (Equation 7 plus Equation 17 and Equation 18).

We can only include the heating and cooling effects of evaporation and capture (Equation 18) as a modification to the models including the suppression factor S, as this is the term the prevents evaporation when the grain temperature is too low and guarantees that $U(t + \Delta t) - kB > 0$. In the next section we illustrate the effects of these various cases, and then in the later sections we will narrow our discussion to comparisons of Case 1 (Planck equilibrium) and Case 4 (stochastically heated, thermally isolated grains). We treat Case 1 as the standard for comparison because almost all studies that set grain temperatures based on the radiation field assume Planck equilibrium temperatures.

The balance between growth and evaporation can be described by two characteristic temperatures. The radiation is characterized by the grain black body temperature, $T_{bb} = (L/16\pi\sigma r^2)^{1/4}$ (Equation 14), which is independent of any dust properties and simply represents the photon energy flux.[3] Almost all the properties of the dust and the spectrum can be encapsulated using an effective evaporation temperature of

$$T_e = -B^{-1} \ln \left(\frac{-\langle dN/dt \rangle_e}{4\pi a^2 A} \right), \tag{19}$$

found by inverting Equation 7 with $S \equiv 1$. For any given spectrum and model for the physics describing the heating of the grains, we can calculate the mapping between the radiative flux characterized by T_{bb} and the evaporation rate, characterized by the effective evaporation temperature, $T_e(T_{bb})$. The gas density implies a critical effective evaporation temperature for growth which is just Equation 17 with $S \equiv 1$. For graphite this becomes

$$T_{crit} = \left[1460 - 360(N-1)^{-1/3}\right] \times \left[1 - (\ln n_5 v_{c1} X_2)/60.8)\right]^{-1} \text{ K} \tag{20}$$

[3] This could also include the geometrical dilution factor, but we do not include it here for simplicity.

and for silicates it becomes

$$T_{crit} = \left[1120 - 330(N-1)^{-1/3}\right] \times \left[1 - (\ln n_5 v_{c1} X_2)/60.9)\right]^{-1} \text{ K} \tag{21}$$

where the density is related to the hydrogen number density n by $\rho = 4nm_p/3$ for roughly Solar abundances. The condition for growth is then simply that $T_{crit} > T_e(T_{bb})$.

If we carry out our simple calculation from §1 for heating grains with mono-energetic photons more carefully, assuming that the grains have a mean temperature $\langle T \rangle$ and are heated to a peak temperature of $T_{peak} = \langle T \rangle + \Delta T$, we find that the effective evaporation temperature is

$$T_e = T_{peak} \left[1 + \frac{T_{peak}}{B} \ln \left(\frac{T_{peak}^3 \Delta T}{S(T_{peak}) \langle T \rangle^4} \right) \right]^{-1}. \tag{22}$$

Because $T_{peak}/B \sim 10^{-2}$ multiplies a logarithm, the effective evaporation temperature is essentially $T_e \simeq T_{peak}$. At large distances $T_{peak} \rightarrow \Delta T$ and for high energy photons ($E_\gamma \gtrsim kB$) we recover the argument in §1 that the evaporation rate does not cut off exponentially at large distances from the source. For low energy photons, the suppression factor becomes exponentially small, the evaporation rate is cut off exponentially at large distances, and we return to the case where stochastic heating is unimportant. In the limit that the grain cools completely between photons, we can calculate the effective evaporation temperature to be

$$T_e = B \left[4 \ln(T_0/T_{bb}) \right]^{-1} \tag{23}$$

where

$$T_0^4 = \frac{A \int B_\nu d\nu}{\sigma \int B_\nu Q_\nu (h\nu)^{-1} N(h\nu)} \tag{24}$$

and $N(h\nu) = 4\pi a^2 \int RS dt$ is the average number of particles that are evaporated after a cold grain absorbs a photon of energy $h\nu$. These equations suggest a functional form for a successful interpolation formula

$$T_e(T_{bb}, T_*) = \frac{\alpha(T_*) + \beta(T_*)\,(T_{bb}/1000 \text{ K})}{1 + \gamma(T_*) \log_{10}(T_{bb}/10 \text{ K})} \tag{25}$$

to the numerical results. We force the fits to agree with Equations 23 and 24 as $T_{bb} \rightarrow 0$ and our Monte Carlo simulations begin to be noisy. We made α, β and γ third order polynomials of the form $\alpha(T_*) = \sum_{i=0}^{3} \alpha_i x^i$ with $x = \log_{10}(T_*/1000 \text{ K})$. These typically fit the $T_e(T_{bb}, T_*)$ curves as a function of T_{bb} and T_* with root mean square residuals of less than 100 K. The resulting fits for thermally isolated, stochastically heated grains (Case 4) are presented in Table 1.

We computed the effective evaporation temperatures for both black bodies and Solar metallicity stellar atmosphere models. For $T_* \geq 3000$ K we used the Castelli & Kurucz (2004) models and for the coldest $T_* = 2600$ K model we used Gustafsson et al. (2008). For cool stars, the harder UV emission may be dominated by hotter chromospheric and coronal regions above the photosphere (e.g., Scalo & Slavsky 1980). These effects could be included by using a higher effective temperature that would mimic these contributions. This temperature can be estimated for any spectrum by matching the values of T_0 in Equation 24.

Although we will not make use of the results in the present paper, we also computed effective evaporation

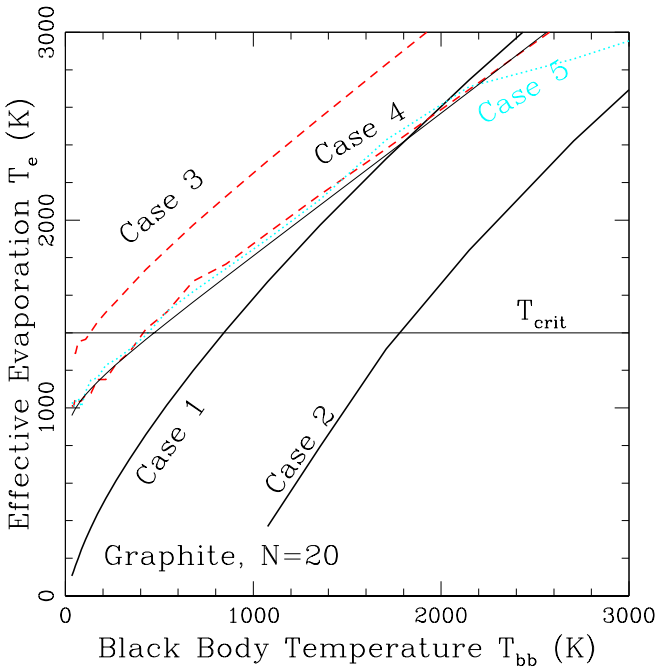

Figure 1. Effective evaporation temperatures, T_e, as a function of the black body temperature, T_{bb}, for a $T_* = 5000$ K black body. A horizontal line shows a typical value of T_{crit} where the grain can start to grow once $T_e < T_{crit}$. The heavy solid lines show the two cases using Planck equilibrium temperatures. Case 1 represents the standard model with $S \equiv 1$, while Case 2 shows the effect of thermally isolating the grains. Case 3 shows the effect of stochastically heating grains in thermal equilibrium with their carrier gas, which leads to a tremendous increase in evaporation rates. Case 4 then adds the suppression factor to thermally isolate the grains, which produces evaporation rates intermediate to Cases 1 and 3. The thin black line shows the analytic approximation to this case using the formula in Table 1. Finally, Case 5 adds the thermal effects of evaporation and capture, which leads to a net reduction in the mean evaporation rate at high temperatures compared to Case 4 because evaporation preferentially occurs when the grain is hot.

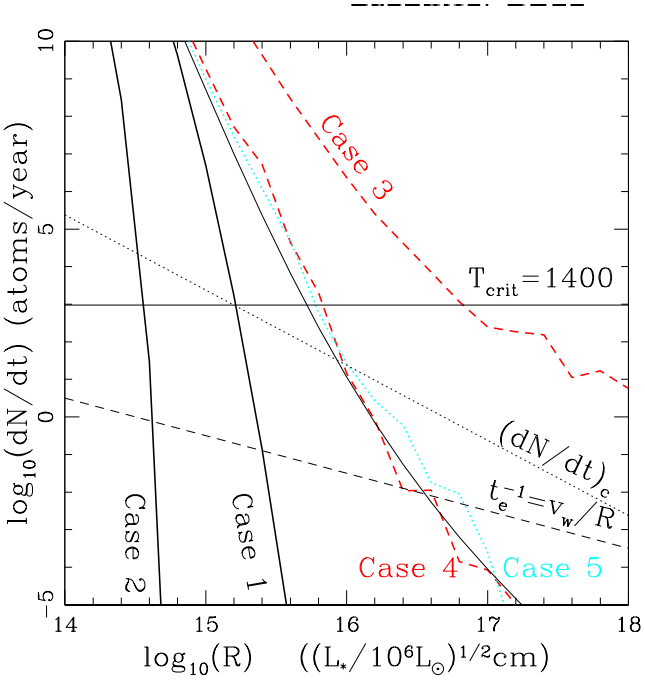

Figure 2. Evaporation rates as a function of radius for a $L_* = 10^6 L_\odot$, $T_* = 5000$ K black body. The Cases are the same as in Figure 1. The horizontal line is the collision rate corresponding to $T_{crit} = 1400$ K, The dotted line labeled $(dN/dt)_c$ shows the collision rate for a wind with $\dot{M} \simeq 2 \times 10^5 M_\odot$ year^{-1} and $v_w = 100$ km/s, and the dashed line labeled $t_e^{-1} = v_w/R$ shows the expansion rate. A grain grows if the collision rate is larger than both the evaporation rate and the expansion rate. Compared to the reference Case 1 (Planck equilibrium), Case 2 (thermal isolation) allows dust formation at much smaller radii and Case 3 (stochastic heating) would allow it only at much larger radii. Case 4, combining both effects, increases the dust formation radius compared to Case 1 by a factor of ~ 4. For the parameter range shown, Case 5 is essentially the same as Case 4. Case 3 would never form dust for this wind density. The radius can be rescaled as $L_*^{1/2}$.

rates for model spectra of supernovae and quasars. We used Type IIP model spectra for days 98 and 197 from Dessart et al. (2013) and Hillier & Dessart (2014, in prep) which are very similar to those of Jerkstrand et al. (2012) at the same phase. This phase corresponds to the early, post-plateau period when the supernova has faded significantly and dust formation becomes possible. For quasars we used the parametrized spectrum of Hönig & Kishimoto (2010). We again truncate the spectra at 13.6 eV. While the harder X-ray photons from the quasar will reach the dust formation region, they transfer little energy to small grains (see Voit 1991, Voit 1992). The net result is that the effective evaporation temperatures for these supernova spectra are roughly those of a $T_* \simeq$ 4000-6000 K star and the quasar is roughly similar to a $T_* \simeq 25000$ K star. For supernova there are additional complications for dust formation in the region where the nuclear decay energy is being absorbed (e.g., Cherchneff & Dwek 2009), but we will consider this problem in a later paper.

3 PHYSICAL RESULTS

Figure 1 shows the effective evaporation temperature $T_e(T_{bb})$ for a 5000 K black body spectrum and graphitic grains with $N = 20$. To guide the eye, we include a line with a constant $T_{crit} = 1400$ K. For a real wind, T_{crit} slowly drops as a function of T_{bb} because of the density dependence in Equation 17, as we will discuss below. For the standard, Case 1, Planck radiative equilibrium model, this grain could begin to grow when the black body temperature dropped to $T_{bb} \simeq 860$ K because the Planck equilibrium temperature of 1400 K is significantly higher than T_{bb} due to the large ratio of $\langle Q_{abs} \rangle / Q_{em}$ for these small grains.

The evaporation rate in Case 1 assumes that the grains are in a thermodynamic bath of the same temperature. On Earth this would be true because the far higher gas densities would keep the grain temperature in collisional equilibrium with the gas temperature on collisional time scales that are short compared to the radiative time scales. In these astrophysical flows, however, the gas collision rate is slow compared to the photon absorption rate or the radiative cooling time scale. Case 2 shows the result of adding the suppres-

sion factor to consider a thermally isolated grain. In this scenario it becomes exceedingly difficult to evaporate anything from a small grain because the enthalpy of the grain does not approach the critical temperature $kB \simeq 7$ eV until $T_g \simeq 2000$ K. As a result, the grain can begin growing at $T_{bb} \simeq 1800$ K.

In Case 3 we modify Case 1 by stochastically heating the grains. This leads to enormously higher evaporation rates for the same energy flux (T_{bb}). A $T_* = 5000$ K black body emits 75% (8%) of its luminosity in photons with energies above 1 eV (3 eV), and these photons can produce $\Delta T \simeq 600$ (1100) K temperature spikes for a $N = 20$ grain starting at $T_g = 0$ K. As a result, the effective evaporation temperature remains high even as T_{bb} drops, and the grain would only be able to start growing at $T_{bb} \simeq 140$ K if T_{crit} is simply held fixed at 1400 K. Case 3 is particularly unphysical because having the grains in thermal equilibrium with the gas essentially assumes that the gas temperature fluctuates in concert with the grain temperature.

In reality, we must make the grains both thermally isolated and stochastically heated, as shown by Case 4. For this radiation temperature, the net effect is still an evaporation rate that is significantly higher than predicted by Case 1. A thin black line underlying the curve shows results for the interpolation formula in Table 1 for this case. As noted in §2, the interpolation formulae are not perfect, as seen here from the small differences in curvature. Nonetheless, where the numerical solution would allow dust formation at $T_{bb} \simeq 430$ K the interpolation formula gives 480 K which corresponds to only a 25% shift in radius.

Finally, Case 4 still lacks the effects of evaporation and condensation on the grain temperature, and this is shown by Case 5. At low temperatures, there is no change from Case 4 because the rate of evaporations and captures is low compared to the rate of photon absorptions. At very high temperatures, the effective evaporation temperature in Case 5 starts to be lower, because evaporation begins to contribute significantly to grain cooling during temperature peaks. This reduces the peak grain temperatures and hence the evaporation rate over Case 4. Essentially, Case 5 starts to approach the fixed temperature of a boiling liquid. However, the differences are only important at such high temperatures that there is no scenario in which the gas densities would be high enough for collision rates to balance evaporation rates.

Figure 2 shows these results translated into rates as a function of radius for a $L_* = 10^6 L_\odot$ source. A horizontal line again shows the constant collision rate corresponding to $T_{crit} = 1400$ K and a grain will grow once the collision rate is higher than the evaporation rate. For fixed T_{crit}, Case 1 reaches this collisional rate at $10^{15.2}$ cm. Case 2, including the suppression factor but not stochastic heating, would drop the formation radius by almost a factor of 5 to $10^{14.6}$ cm. Case 3, adding stochastic heating without the suppression factor, would increase the formation radius compared to Case 1 by almost a factor of 50 to $10^{16.9}$ cm. At the largest radii, the slope of the evaporation rate curve for this case has converged to the $\langle dN/dt \rangle_e \propto r^{-2}$ scaling predicted in §1. Case 4, with both stochastic heating and the suppression factor, leads to a radius roughly 4 times larger than in Case 1, at $10^{15.8}$ cm. Case 5, where we had the heating and cooling from evaporation and capture, is little different from Case 4 over the parameter range shown in Figure 2. Given

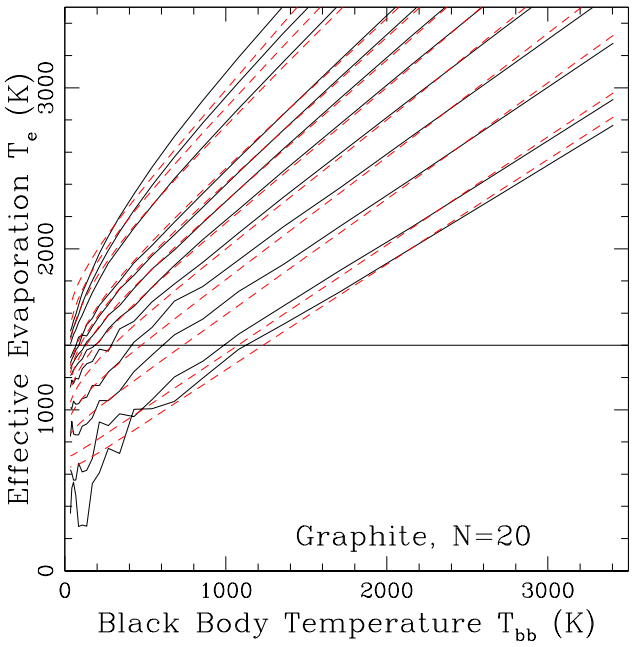

Figure 3. The Case 4 effective evaporation temperature, T_e, as a function of the black body temperature, T_{bb}, for (from bottom to top) $T_* = 2600$, 3000, 4000, 5000, 6000, 7000, 8000, 9000, 10000, 15000, 20000 and 30000 K black bodies and $N = 20$ graphitic grains. The solid lines are the numerical results and the dashed lines are the results using the approximation formula for this case from Table 1. The root mean square difference between the two is 80 K, which is partly due to the order of the approximation and partly due to the noise in the Monte Carlo results at low T_{bb} and T_*.

the interpolation formula for $T_e(T_{bb})$, the evaporation rate is simply $4\pi a^2 A \exp(-B/T_e(T_{bb}))$ and a thin black line shows that this model recreates the numerical results reasonably well.

In practice, the collision rate (Equation 4) and the required T_{crit} vary with radius because of the changing density of a wind. To illustrate this, Figure 2 also shows the collision rate $(dN/dt)_c$ for a wind with $\dot{M} \simeq 2 \times 10^{-5} M_\odot$ year^{-1}, $v_w = 100$ km/s and $X = 0.01$. This was chosen so that it passes through the point at $R \simeq 10^{15.2}$ cm where the Case 1 evaporation rate has $T_{crit} = 1400$ K. The collision rate simply declines with the density as $(dN/dt)_c \propto R^{-2}$ which translates into $T_{crit} = 1730$, 1560, 1430, 1310, and 1210 K at $R = 10^{14}$, 10^{15}, 10^{16}, 10^{17} and 10^{18} cm. Compared to a fixed T_{crit} (density), the dust formation radius becomes slightly smaller for Case 2 and slightly larger for Cases 4 and 5. For Case 3, however, the evaporation rate is above the collision rate at all radii and no dust would form in this case. Also shown is the expansion rate, $t_e^{-1} = v_w/R$, which determines the minimum mass loss rate for dust formation. If the density is so low that the collision rate is below t_e^{-1}, the grain has no further collisions and stops growing.

We will now only focus on the differences between Case 1, representing the standard Planck radiative equilibrium model, and Case 4. We do not discuss Cases 2 and 3 further because they are not physical, and Case 5 differs from Case 4 only under physical conditions that do not seem to be rel-

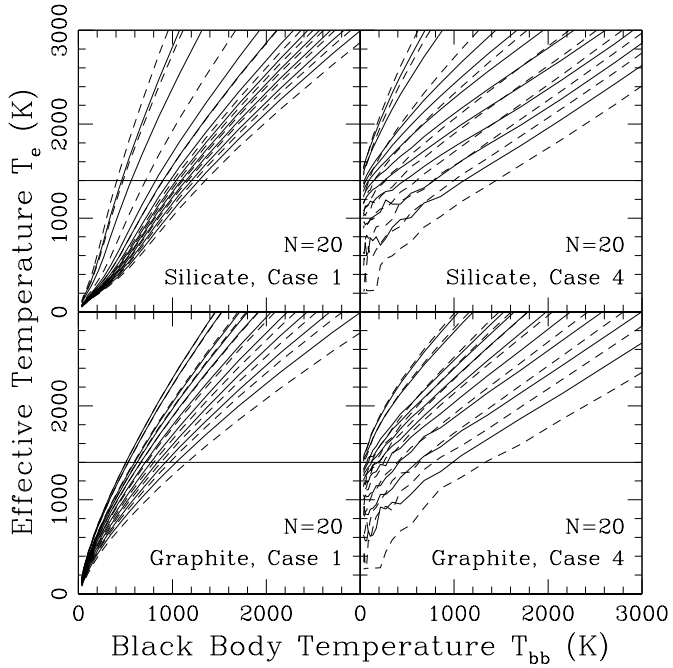

Figure 4. The effective evaporation temperature, T_e as a function of T_{bb} for $N = 20$ graphitic (top) and silicate (bottom) grains with radiation temperatures (from bottom to top) of $T_* = 2600$, 3000, 4000, 5000, 6000, 7000, 8000, 9000, 10000, 15000, 20000 and 30000 K. The horizontal line at $T_{crit} = 1400$ K corresponds to a typical collision rate. The solid lines are for black bodies and the dashed lines are for stellar atmosphere models. The left panels show the Planck equilibrium results (Case 1) and the right panels show the results for stochastically heated, thermally isolated grains (Case 4).

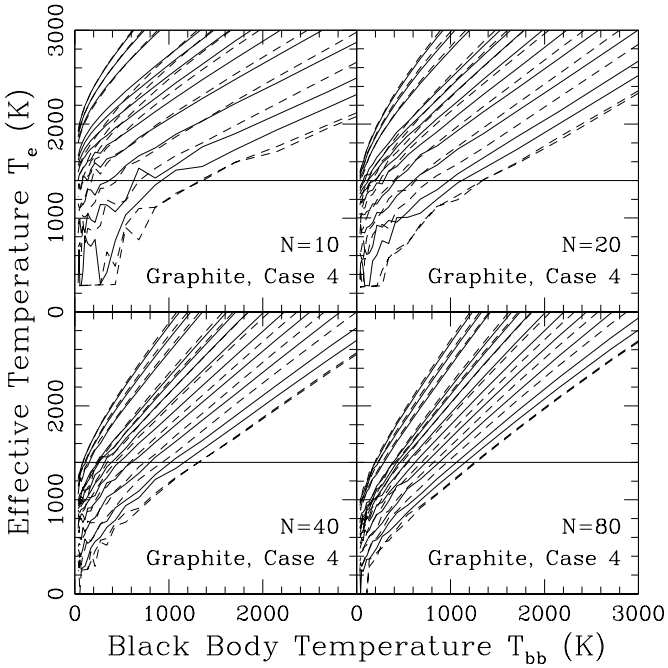

Figure 5. The effective evaporation temperature, T_e as a function of T_{bb} for stochastically heated, thermally isolated (Case 4) $N = 10$ (top left), 20 (top right), 40 (lower left) and 80 (lower right) graphitic grains The range of radiation temperatures is the same as in Figure 4 for both black bodies (solid) and stellar atmospheres (dashed). The horizontal line at $T_{crit} = 1400$ K corresponds to a typical collision rate.

evant for dust formation. Figure 3 shows the full suite of graphitic Case 4 $N = 20$ black body models models and the interpolated model from Table 1 for radiation temperatures from $T_* = 2600$ K to 30000 K. The overall rms residual is 80 K, partly due to systematic mismatches and partly due to noise for the low T_{bb} and T_* cases. Most of the differences can be thought of as small mismatches ($\sim 10\%$) in the meaning of T_* between the numerical models and the approximations. Since it is unlikely that these approximations will ever be used in situations where the temperature is that well known, and because of the additional uncertainties in the input dust physics, there seemed no need to develop still more complicated approximations that would significantly reduce the residuals. The results for the other models are similar, so we will not show further comparisons of the numerical results and the approximations.

Figure 4 shows the Case 1 and Case 4 results for both graphitic and silicate $N = 20$ grains, both black bodies and model atmospheres, and as a function of radiation temperature T_*. A constant $T_{crit} = 1400$ K line again provides a comparison. Without stochastic heating, the effective evaporation temperature does depend on T_* in the sense that T_e increases with T_* at all fluxes. This is simply driven by the rise in $\langle Q_{abs} \rangle$ with T_*. The trends are relatively smooth except for a faster rise for silicate grains and high T_* created by the jump in Q_{abs} near $\lambda \simeq 0.2\mu$m. At low temperatures, stellar atmosphere models have lower T_e for fixed T_* because

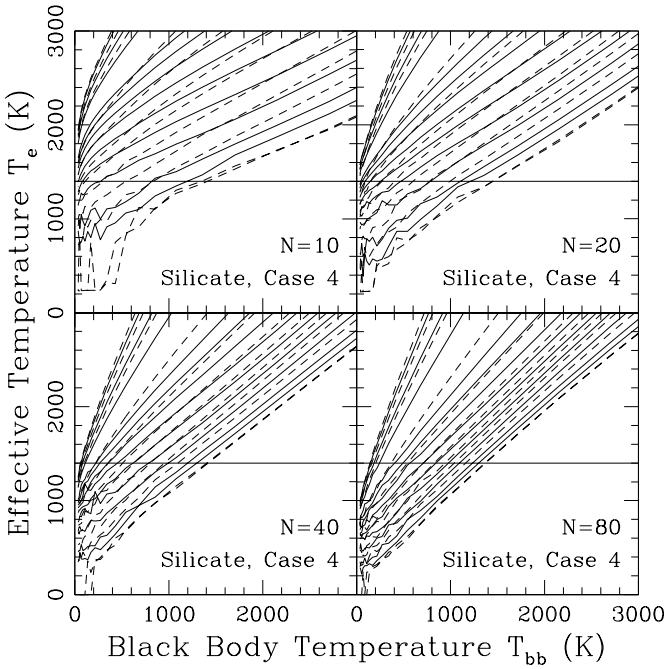

Figure 6. As in Figure 5, but for silicate grains.

of strong atmospheric absorption at shorter wavelengths for cooler stars. The effect becomes smaller for hotter stars because the spectral breaks become weaker.

For the coolest stars, the additional physical effects essentially cancel to leave little difference between Case 1 and Case 4. For the $T_* = 2600$ K stellar atmospheres, the silicate grains have $T_e = 1400$ K at $T_{bb} \simeq 1400$ K in both cases, while for the graphitic grains the temperature rises modestly from $T_{bb} \simeq 1200$ to 1400 K, which means the grain would actually start to grow sooner than in Case 1. However, even for moderately higher radiation temperatures, Case 4 requires substantially lower radiation fluxes (T_{bb}) for the same evaporation rate. We have already discussed the $T_* = 5000$ K case in detail, and for higher radiation temperatures the differences become still more extreme. Figures 5 and 6 show the changes in T_e with grain size for $N = 10$, 20, 40 and 80. Not surprisingly, the effects of stochastic heating are stronger for smaller grains and weaker for larger grains. While we do not show the comparisons, the Case 4 results increasingly resemble the Case 1 results as N increases, although even for $N = 80$ there are significant differences and the differences become larger for higher radiation temperatures.

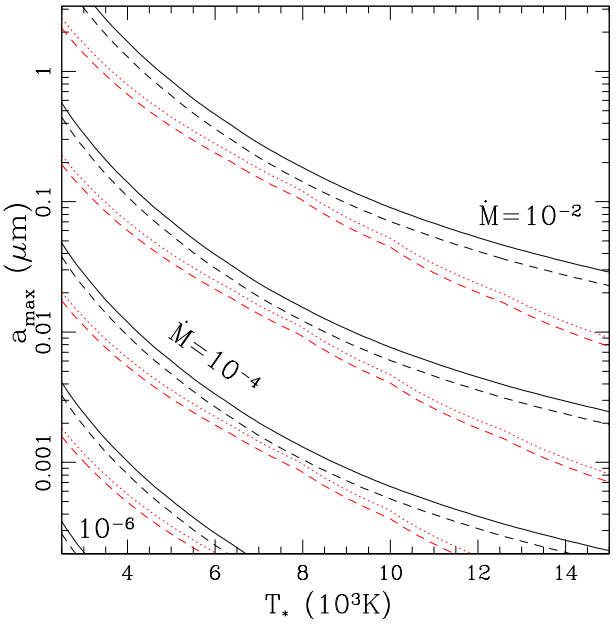

Figure 7. Final grain sizes a_{max} assuming Planck equilibrium temperatures (Case 1) and black body spectra as a function of stellar temperature. The solid black (dotted red) curves are for graphite (silicate) grains and $L_* = 10^4 L_\odot$. The adjacent but slightly lower black (red) dashed curves are for graphite (silicate) and $L_* = 10^6 L_\odot$. The mass loss rates, from largest to smallest final sizes, are $\dot{M} = 10^{-2}$, 10^{-3}, 10^{-4}, 10^{-5} and $10^{-6} M_\odot$/year with the dependencies on other variables discussed in the text. The nominal case is $N = 20$ with $\alpha = 1$, $\beta = 1$, $X = 0.005$, $v_c = 1$ km/s and $M_* = 10 M_\odot$.

4 DUST FORMATION IN WINDS

For a steady wind we can integrate Equation 4 from the radius R_f where the growth rate begins to exceed the evaporation rate to determine the typical final grain size. If we scale the wind velocity by the escape velocity (Equation 2) then

$$a_{max} = \frac{\alpha X \dot{M} v_c}{32\pi G M_* \rho_b \beta^2} \left(\frac{T_{bb}}{T_*}\right)^2 \simeq 0.16 \frac{\alpha X_2 \dot{M}_4 v_{c1}}{\beta^2 M_{*10} \rho_{b3}} \left(\frac{T_{bb}}{T_*}\right)^2 \ \mu\mathrm{m} \quad (26)$$

where the formation radius is characterized by the black body temperature T_{bb} at which the grains can begin to grow. In order to be considered a dust particle, this final size must contain some minimum number of particles, $N_{min} = 10 N_{min10}$, which implies a minimum mass loss rate

$$\begin{aligned} \dot{M} &> 8 \left(6\pi^2 N_{min} m_0 \rho_b^2\right)^{1/3} \frac{G M_* \beta^2}{\alpha X v_c} \left(\frac{T_*}{T_{bb}}\right)^2 \quad (27) \\ &\gtrsim 6 \times 10^{-8} \frac{N_{min10}^{1/3} M_{*10} \beta^2}{\alpha v_{c1} X_2} \left(\frac{T_*}{T_{bb}}\right)^2 \ M_\odot/\mathrm{year}, \end{aligned}$$

below which the growth of the grain is prevented by the kinetics of the collisional process. Note that to lowest order, the final dust properties are independent of the stellar luminosity and are largely controlled by $\dot{M}$ and the temperature ratio T_{bb}/T_*. Since the black body temperature T_{bb} at which dust formation begins also is a function of T_*, the dependence of the dust properties on T_* is even stronger than the explicit quadratic.

Equation 26 does not represent a true model of a dust accelerated wind because we are primarily interested in dust formation in stellar eruptions, supernovae or AGN where the dust is not responsible for accelerating the gas to produce the outflow. Despite ignoring the problem of self-consistently accelerating a dusty wind, the simple model based on Equation 26 produces quite reasonable results. For example, if we simply apply Equation 26 with $X = 0.0046$, $M_* = 1 M_\odot$ and $L_* = 2 \times 10^4 L_\odot$ to match the $\epsilon_c/\epsilon_0 = 1.6$ case of Gail & Sedlmayr (1985), we find $a_{max} = 0.006$, 0.15 and

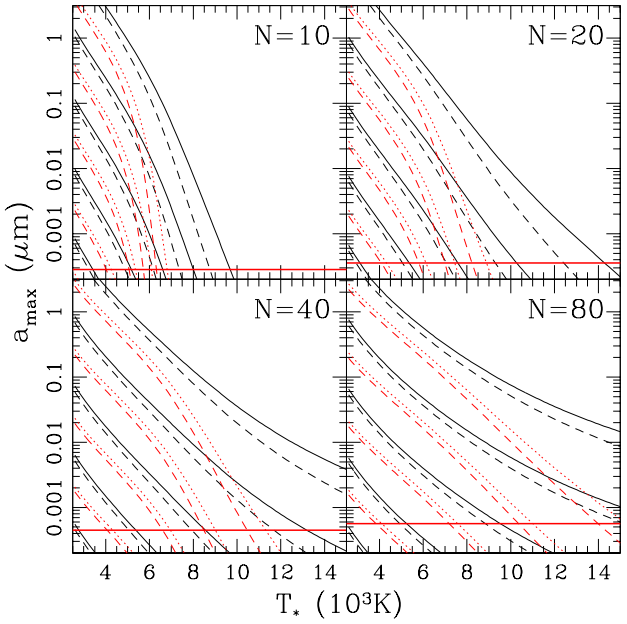

Figure 8. Final grain sizes a_{max} assuming stochastically heated, thermally isolated grains (Case 4) and stellar atmospheres as a function of stellar temperature for the $N = 10$ (top left), 20 (top right) 40 (lower left) and 80 (lower right) cases. The solid black (dotted red) curves are for graphite (silicate) grains and $L_* = 10^4 L_\odot$. The adjacent but slightly lower black (red) dashed curves are for graphite (silicate) and $L_* = 10^6 L_\odot$. The mass loss rates and parameters other than N are as in Figure 7. The heavy horizontal line shows the size of an N particle grain.

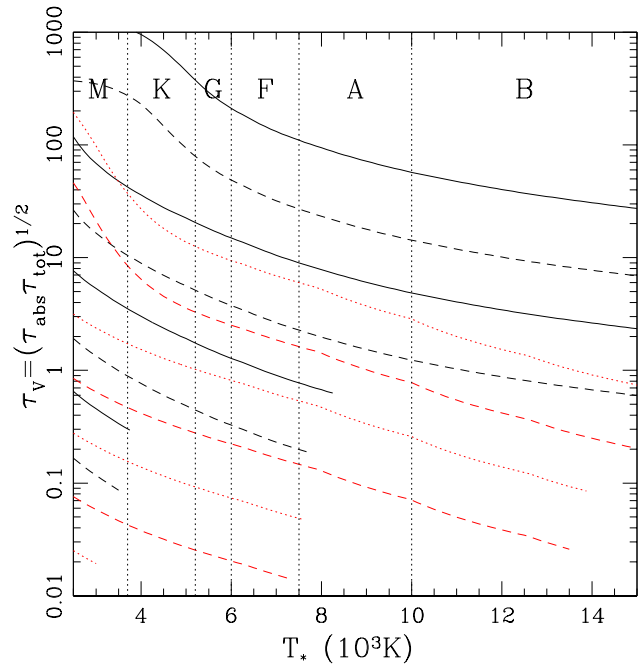

Figure 9. Wind optical depths at V-band assuming Planck equilibrium (Case 1). The solid black (dotted red) curves are for graphite (silicate) grains and $L_* = 10^4 L_\odot$. The adjacent but lower black (red) dashed curves are for graphite (silicate) and $L_* = 10^6 L_\odot$. The mass loss rates, from largest to smallest optical depth, are $\dot{M} = 10^{-3}$, 10^{-4}, 10^{-5} and $10^{-6} M_\odot$/year with the dependencies on other variables discussed in the text. The nominal case is $N = 20$ and the curves are truncated when a_{max} corresponds to $N = 20$.

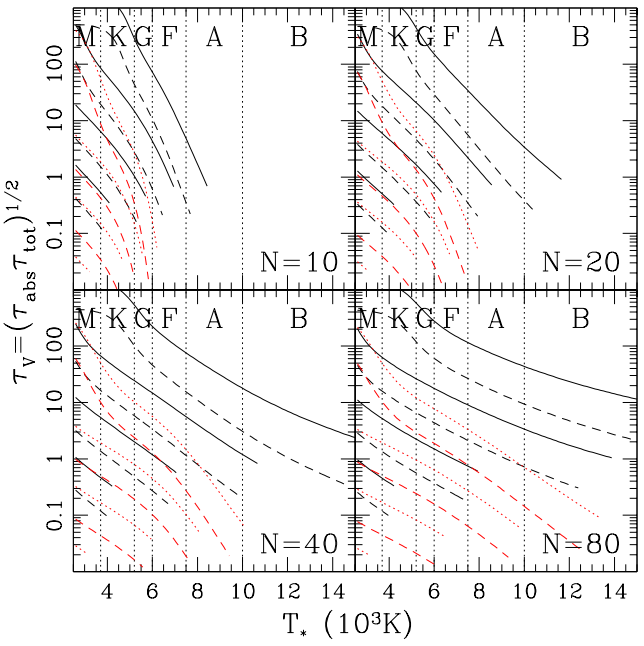

Figure 10. Wind optical depths at V-band assuming thermally isolated, stochastically heated grains (Case 4) for $N = 10$, 20, 40 and 80. The solid black (dotted red) curves are for graphite (silicate) grains and $L_* = 10^4 L_\odot$. The adjacent but lower black (red) dashed curves are for graphite (silicate) and $L_* = 10^6 L_\odot$. The mass loss rates, from largest to smallest optical depth, are $\dot{M} = 10^{-3}$, 10^{-4}, 10^{-5} and $10^{-6} M_\odot$/year with the dependencies on other variables discussed in the text. The curves are terminated when a_{max} corresponds to N particles.

0.84μm, compared to 0.013, 0.031 and 0.13μm in the full calculations for $\dot{M} = 10^{-6}$, 2×10^{-5} and $2 \times 10^{-4} M_\odot$ year. This also assumed $\beta = 1$, $v_c = 1$ km/s, $T_* = 2600$ K and Planck equilibrium (Case 1). The agreement is relatively good, and the differences are likely due to ignoring the effect of the dust on the radiation field. Once the dust has an appreciable optical depth, Equation 15 is incomplete because as the newly formed dust begins to trap some of the radiation, the temperatures rise and the dust formation radius is driven outwards leading to smaller final grain sizes. In experiments with DUSTY (Ivezic & Elitzur 1997, Ivezic et al. 1999), we found that the formation radius increases roughly as $R_f \propto (1 + \tau_V)^{0.2}$ due to this effect. For $\tau_V \simeq 100$, like the $\dot{M} = 2 \times 10^{-4} M_\odot$ year model from Gail & Sedlmayr (1985), this would lead us to overestmate the grain size by a factor of 2-3, accounting for much of the difference in the estimates. This effect is not critical to the discussion which follows, because it only becomes important once dust forms with an appreciable optical depth, and we are mainly concerned with the question of whether dust forms at all.

Figure 7 shows the dependence of a_{max} on mass loss rates and stellar temperature using Planck equilibrium temperatures (Case 1) and black bodies. Figure 8 shows the results for stochastically heated, thermally isolated grains (Case 4) and stellar atmospheres. For the Planck equilibrium case we only show $N = 20$ because the other cases will be almost identical. These results use $X \equiv 0.005$, $\beta = 1$, $\alpha \equiv 1$, $v_c \equiv 1$ km/s and $M_* \equiv 10 M_\odot$. To first order, the final grain size simply scales as in Equation 26 but there is a secondary, logarithmic effect from the dependence of T_{crit} on the variable combination $X\dot{M}v_c/\beta M_*^{1/2} L_*^{3/4}$ (Equations 21 and 22). We illustrate these effects by showing the results for $L_* = 10^4$ and $10^6 L_\odot$.

If we compare Figure 7 and 8, we see that many LBVs and all yellow supergiants in their hotter states could form dust if we consider Case 1 (Figure 7). However, particularly for the oxygen rich, silicate chemistry usually associated with the winds of massive stars, they cannot do so if we consider Case 4 (Figure 8). There is some ambiguity as to the appropriate N, but essentially any of the four cases shown will reproduce the observed behavior. As hot O/B (LBV) or A (yellow supergiants) stars, it is impossible for these stars to form dust even at mass loss rates near $\dot{M} \sim 10^{-4} M_\odot$/year. When LBVs enter their eruptive states, the wind becomes (non-dust) optically thick and the stellar photosphere is shielded by a pseudo-photosphere created by the wind leading to the apparent temperature of an F star ($T_* \sim 7500$ K, Davidson 1987) and at this radiation temperature it becomes possible to form dust (Kochanek 2011). Similarly, in their cooler states, the yellow hypergiants appear as cooler G/F stars and also enter the regime where dust formation is allowed. Particularly for the yellow hypergiants it is very difficult to understand the lack of dust formation in their hotter phases without this mechanism.

We can also estimate the resulting optical depth assuming that at every radius all the condensible material is in grains of size $a = a_{max}(1 - R_f/R)$ found by integrating Equation 4 starting at the formation radius R_f where growth begins. This is slightly inconsistent because it assumes monomer growth and a constant collision velocity – for example, if all grains are in grains of size a than growth is really be coagulation with a geometric cross section of $4\pi a^2$

rather than πa^2. Similarly, sticking probabilities and collision velocities will also change. However, the biggest uncertainty is how many grains are initially formed to begin growing, which we encapsulate as the fraction f of the condensible material that is ultimately incorporated into grains (see, e.g., the discussion in Ferrarotti & Gail 2006). Recent detailed simulations by Nanni et al. (2013) and Ventura et al. (2014) find condensed fractions of order $f \sim 0.1$ to 0.5. The dust represents mass fraction Xf of the total wind mass. Observationally, this is roughly $Xf \sim 1/200$ to $1/400$ for Galactic sources (e.g., Knapp 1985). Since we have scaled our results to $X = 0.005 = 1/200$ typical values of f should be in the range $0.5 \lesssim f \lesssim 1$.

Under these assumptions, the opacity is just $\kappa = 3fXQ/4\rho_b a$, so the optical depth is

$$\tau = \frac{3fv_w}{\alpha v_c} \int_0^{a_{max}} Q(a) da/a \tag{28}$$

after converting the radial integral into one over the grain size. When the grains are small, Q/a is nearly constant, so the optical depth simply grows $\propto a_{max}$. It rises more steeply for $0.1 < a_{max} < 1\mu$m and then flattens for still larger grains. In any dust forming flow there should always be a strong correlation of optical depth with maximum grain size. Note that since $a_{max} \propto v_w^{-2}$, the optical depth does decrease with increasing wind velocity despite the leading factor of v_w in Equation 28. We estimate the effective absorption optical depth as $\tau = (\tau_{abs}\tau_{tot})^{1/2}$ where $\tau_{tot} = \tau_{abs} + \tau_{sca}$ combines the absorption and scattering optical depths.

Figure 9 shows the resulting visual optical depths assuming Planck equilibrium (Case 1) as a function of stellar temperature, luminosity and mass loss rate. We assume $f = 1$ and truncate the results when a_{max} corresponds to a grain with $N < 20$ particles. For a given mass loss rate, optical depths are highest for colder, lower luminosity stars and graphitic dusts. Figure 9 shows mass loss rates of $\dot{M} = 10^{-6}$, 10^{-5}, 10^{-4} and $10^{-3} M_\odot$/year covering the range from stellar winds to the mass loss rates invoked for SN impostors or to explain the superluminous Type IIn SNe (e.g., Ofek et al. 2014). Without the effects of stochastic heating, most high mass loss transients would be completely opaqued as soon as dust formation becomes feasible. Note, however, that other than hotter stars requiring higher minimum mass loss rates, there is nothing special about the stellar temperature.

Figure 10 shows the results for thermally isolated, stochastically heated grains (Case 4) as a function of the limiting particle size N. Particularly for the smaller N cases, the expected optical depth drops sharply as the stellar temperatures rise, and dust formation simply does not occur for hotter stars and the mass loss rates of even very dense winds. Silicate dusts in particular show an abrupt cutoff at $T_* \sim 7000$ K. At very low temperatures, the optical depths are slightly enhanced because the thermal isolation allows dust formation to begin earlier, as discussed in §3, although this neglects the physics of accelerating true dust driven winds.

5 DISCUSSION

Dust formation is a balance between growth by collisions and evaporation. The evaporation rate is set by the grain temperature and the grain temperature is almost always controlled by radiative heating and cooling rather than gas collisions. For small grains, this temperature is stochastic and driven by the flux of soft UV photons, just as in the interstellar medium. Thus, dust formation is far more dependent on the spectrum of the radiation field than would be predicted simply using equilibrium temperatures. While Planck factors and stellar wind speeds disfavor dust formation around hot stars, all stars with $T_* \lesssim 15000$ K and $\dot{M} \gtrsim 10^{-5} M_\odot$/year should have winds with significant visual optical depths $\tau_V \gtrsim 0.1$ if there were no additional physics.

Stochastic heating provides that extra physics because the abundance of soft UV photons grows (initially) exponentially with stellar temperature. For a cold AGB star, stochastic heating is almost irrelevant, but is is already important for G/F stars, A stars can only form dust if $\dot{M} \gtrsim 10^{-4} M_\odot$/year, and B stars cannot form dust. These limits are stronger for silicate dusts because they have lower evaporation temperatures. The primary result from this paper is the set of approximations presented in Table 1 for the effective evaporation temperatures (Equation 19) of small grains as a function grain size N, radiative flux as characterized by T_{bb} (Equation 15) and the radiation temperature T_*. Combined with the critical temperatures defined by Equations 21 and 22, these can be used to better estimate whether dust formation can occur and the radius or time at which it commences. Note that the apparent temperature of the newly forming dust will be high because most of the emission occurs during the temperature spikes rather than the cooler phases.

The role of stochastic heating in dust formation naturally explains the episodic dust formation of LBV stars and OH/IR stars (Kochanek 2011). At some phases, these stars appear as hotter B or A stars, respectively, and cannot form dust despite their high mass loss rates. At some phases they appear as cooler G/F stars and form large quantities of dust. For OH/IR stars this involves only modest changes in luminosity and mass loss rates. In the (great) eruptions of LBVs, there is a large change in luminosity and mass loss rates, but the higher mass loss rate matters more because it allows a lower temperature pseudo-photosphere to form in the wind (Davidson 1987) than because the higher wind density increases collisional growth rates.

As discussed by Johnson et al. (1993) there are ultimately problems with simply extrapolating these approaches to very small N. This has been discussed most extensively for polycyclic aromatic hydrocarbons (PAHs) in the interstellar medium (e.g., Omont 1986). The physics of evaporation is roughly correct for all N since is based on a quantum mechanical view of vibrational modes, but the binding energies of carbon atoms in a small molecule are stronger than for bulk graphite. The real break down is in the extrapolation of the radiation absorption cross sections to small N. Grains absorb at "all" wavelengths, while simple molecules absorb only at discrete wavelengths. For example, the electronic transition absorption cross sections of PAHs and carbon clusters calculated by Malloci et al. (2007) begin to break up into discrete bands for $N < 10$, with peaks that are comparable to extrapolating the bulk Q but now with significant gaps. Effectively, as N becomes smaller, Q will

decline faster than a, allowing the formation of molecules but preventing their growth into macroscopic grains.

Our ultimate goal for these calculations is to examine dust formation in other environments where the radiation field is very different from that of cool (AGB) stars. For example, there are models which propose that dust forms in outflows from quasar accretion disk (e.g., Elvis et al. 2002 Czerny & Hryniewicz 2011). But the UV radiation field of a quasar has the equivalent stochastic heating power of a $T_* = 25000$ K star even after cutting off all radiation above 13.6 eV, and this probably make dust formation in such outflows impossible. This is already implicit in models using these effects to destroy PAHs in dust near quasars in order to explain the lack of PAH features in quasar dust spectra (see, e.g., Voit 1991, Voit 1992).

Supernovae have softer spectra, but their typical radiation temperatures correspond to $T_* \simeq$ 4000-6000 K, a regime where small changes in radiation temperature have a major impact on dust formation. This may be related to the contradictory evidence about whether supernovae are a significant source of dust – many show no evidence for significant dust formation, while some clearly produce large quantities of dust (see the review in Gall et al. 2011). The stellar transients called supernova "impostors" (see the recent studies by Smith et al. (2011) and Kochanek et al. (2012)) and the pre-supernova outbursts associated with some Type IIn supernovae or needed to provide the massive shells proposed to power superluminous Type IIn supernovae (see, e.g., Ofek et al. 2014) also have radiation temperatures in this regime, so dust formation should be a powerful probe of the amount of ejected mass.

ACKNOWLEDGMENTS

I would like to thank T. Miller, T. Thompson and B. Wyslouzil for valuable discussions.

REFERENCES

Bianchi, S., & Schneider, R. 2007, MNRAS, 378, 973
Castelli, F., & Kurucz, R. L. 2004, arXiv:astro-ph/0405087
Cherchneff, I., & Dwek, E. 2009, ApJ, 703, 642
Clayton, D. D., & Wickramasinghe, N. C. 1976, Ap&SS, 42, 463
Czerny, B., & Hryniewicz, K. 2011, A&A, 525, L8
Davidson, K. 1987, ApJ, 317, 760
Deguchi, S. 1980, ApJ, 236, 567
Dessart, L., Hillier, D. J., Waldman, R., & Livne, E. 2013, MNRAS, 433, 1745
Desert, F. X., Boulanger, F., & Shore, S. N. 1986, A&A, 160, 295
Donn, B., & Nuth, J. A. 1985, ApJ, 288, 187
Draine, B. T., & Lee, H. M. 1984, ApJ, 285, 89
Draine, B. T., & Anderson, N. 1985, ApJ, 292, 494
Draine, B. T. 1995, Ap&SS, 233, 111
Dwek, E. 1988, ApJ, 329, 814
Elvis, M., Marengo, M., & Karovska, M. 2002, ApJL, 567, L107
Ferrarotti, A. S., & Gail, H.-P. 2006, A&A, 447, 553
Gail, H.-P., Keller, R., & Sedlmayr, E. 1984, A&A, 133, 320
Gail, H.-P., & Sedlmayr, E. 1985, A&A, 148, 183
Gail, H.-P., & Sedlmayr, E. 1988, A&A, 206, 153
Gail, H.-P., & Sedlmayr, E. 2013, Physics and Chemistry of Circumstellar Dust Shells, by Hans-Peter Gail , Erwin Sedlmayr, Cambridge, UK: Cambridge University Press, 2013
Gall, C., Hjorth, J., & Andersen, A. C. 2011, A&ARv, 19, 43
Gauger, A., Sedlmayr, E., & Gail, H.-P. 1990, A&A, 235, 345
Guhathakurta, P., & Draine, B. T. 1989, ApJ, 345, 230
Gustafsson, B., Edvardsson, B., Eriksson, K., et al. 2008, A&A, 486, 951
Hönig, S. F., & Kishimoto, M. 2010, A&A, 523, A27
Humphreys, R. M., & Davidson, K. 1994, PASP, 106, 1025
Ivezic, Z., & Elitzur, M. 1997, MNRAS, 287, 799
Ivezic, Z., Nenkova, M., & Elitzur, M. 1999, User Manual for DUSTY, University of Kentucky Internal Report http:www.pa.uky.edu̅moshedusty
Jerkstrand, A., Fransson, C., Maguire, K., et al. 2012, A&A, 546, A28
Johnson, D. J., Friedlander, M. W., & Katz, J. I. 1993, ApJ, 407, 714
Keith, A. C., & Lazzati, D. 2011, MNRAS, 410, 685
Knapp, G. R. 1985, ApJ, 293, 273
Kochanek, C. S. 2011, ApJ, 743, 73
Kochanek, C. S., Szczygieł, D. M., & Stanek, K. Z. 2012, ApJ, 758, 142
Kozasa, T., Hasegawa, H., & Nomoto, K. 1991, A&A, 249, 474
Kwok, S. 1975, ApJ, 198, 583
Lafon, J.-P. J., & Berruyer, N. 1991, A&ARv, 2, 249
Laor, A., & Draine, B. T. 1993, ApJ, 402, 441
Lefevre, J. 1979, A&A, 72, 61
Malloci, G., Joblin, C., & Mulas, G. 2007, Chemical Physics, 332, 353
Nanni, A., Bressan, A., Marigo, P., & Girardi, L. 2013, MNRAS, 434, 2390
Netzer, N., & Elitzur, M. 1993, ApJ, 410, 701
Nozawa, T., Kozasa, T., Umeda, H., Maeda, K., & Nomoto, K. 2003, ApJ, 598, 785
Ofek, E. O., Sullivan, M., Shaviv, N. J., et al. 2014, arXiv:1401.5468
Omont, A. 1986, A&A, 164, 159
Rowan-Robinson, M., & Harris, S. 1983, MNRAS, 202, 797
Salpeter, E. E. 1977, ARA&A, 15, 267
Scalo, J. M., & Slavsky, D. B. 1980, ApJL, 239, L73
Sellgren, K. 1984, ApJ, 277, 623
Smith, N., Li, W., Filippenko, A. V., & Chornock, R. 2011, MNRAS, 412, 1522
Todini, P., & Ferrara, A. 2001, MNRAS, 325, 726
Ventura, P., Dell'Agli, F., Schneider, R., et al. 2014, MNRAS, 439, 977
Vink, J. S. 2012, Astrophysics and Space Science Library, 384, 221
Voit, G. M. 1991, ApJ, 379, 122
Voit, G. M. 1992, MNRAS, 258, 841
Waxman, E., & Draine, B. T. 2000, ApJ, 537, 796
Wölk, J., Strey, R., Heath, C.H., & Wyslouzil, B., 2002, J Chem Phys, 117, 4954

Table 1. Fitting Formulas for the Effective Evaporation Temperature

Spectrum	Dust	N	Term	Coefficients (α_i, β_i, γ_i)			
BB	Gra	10	α	390.842	1018.267	−0.541	−0.406
			β	1.386	−2.373	1.182	0.016
			γ	$6.3f$	−0.279	0.869	−0.639
BB	Sil	10	α	511.015	869.375	−0.390	−0.126
			β	1.158	−2.059	0.919	0.082
			γ	$6.3f$	−0.193	0.613	−0.376
BB	Gra	20	α	315.666	804.721	−0.569	−0.249
			β	1.718	−2.566	0.962	0.199
			γ	$6.3f$	−0.329	0.939	−0.642
BB	Sil	20	α	319.523	816.994	−0.425	−0.171
			β	1.686	−2.443	0.434	0.550
			γ	$6.3f$	−0.265	0.710	−0.383
BB	Gra	40	α	218.575	665.769	−0.453	−0.241
			β	2.006	−2.672	0.654	0.351
			γ	$6.3f$	−0.357	0.959	−0.605
BB	Sil	40	α	119.764	784.284	−0.354	−0.148
			β	2.260	−2.918	0.006	0.952
			γ	$6.3f$	−0.350	0.851	−0.428
BB	Gra	80	α	150.741	570.282	−0.471	−0.195
			β	2.185	−2.646	0.445	0.447
			γ	$6.3f$	−0.368	0.936	−0.554
BB	Sil	80	α	−34.368	752.842	−0.400	−0.111
			β	2.658	−3.106	−0.326	1.281
			γ	$6.3f$	−0.378	0.818	−0.340
Star	Gra	10	α	−143.151	1397.619	−0.417	−0.159
			β	1.773	−2.638	0.555	0.459
			γ	$6.3f$	−0.449	1.296	−0.938
Star	Sil	10	α	−110.286	1360.755	−0.408	−0.168
			β	2.015	−2.901	0.262	0.698
			γ	$6.3f$	−0.431	1.095	−0.635
Star	Gra	20	α	−85.472	1082.070	−0.484	−0.138
			β	2.102	−2.947	0.255	0.744
			γ	$6.3f$	−0.488	1.367	−0.941
Star	Sil	20	α	−155.750	1160.095	−0.518	−0.128
			β	2.494	−3.345	−0.152	1.123
			γ	$6.3f$	−0.488	1.203	−0.672
Star	Gra	40	α	−44.395	861.750	−0.420	−0.124
			β	2.333	−3.030	0.018	0.865
			γ	$6.3f$	−0.498	1.335	−0.863
Star	Sil	40	α	−330.717	1155.925	−0.362	−0.029
			β	3.064	−3.813	−0.700	1.683
			γ	$6.3f$	−0.556	1.303	−0.686
Star	Gra	80	α	−93.857	783.889	−0.410	−0.191
			β	2.537	−3.040	0.035	0.846
			γ	$6.3f$	−0.509	1.285	−0.796
Star	Sil	80	α	−330.207	1006.511	−0.428	−0.215
			β	3.198	−3.652	−0.547	1.632
			γ	$6.3f$	−0.452	0.825	−0.195

Note. — The Spectrum, Dust and N columns indicate the input spectrum (black body or stellar atmosphere), the type of dust (Graphitic or silicate) and the number of particles in the grain. The Term column is the coefficient in the fitting formula Equation 25 where the four coefficients for $\alpha(T_*)$, $\beta(T_*)$ and $\gamma(T_*)$ are to be summed as $\alpha(T_*) = \sum_{i=0}^{3} \alpha_i x^i$ with $x = \log_{10}(T_*/1000\ \mathrm{K})$. They are valid for $2600 < T_* < 30000$ K with a typical rms residual compared to the numerical results of < 100 K in the estimate of T_e, including the noise in the numerical results. Most systematic residuals can be viewed as ~ 500 K uncertainties in the appropriate T_*.